Personalized tDCS targeting visual motion area V5 modulates smooth pursuit initiation

Short title: Personalized tDCS targeting V5 modulates pursuit

Radecke, Jan-Ole[a,b,*], Kühn, Alexander[a,b], Erdbrügger, Tim[c,d], Buschermöhle, Yvonne[c,e], Rashidi, Sogand[a,b], Stöckler, Hannah[a,b], Sack, Benjamin[a,b], Borgwardt, Stefan[a,b], Schneider, Till R.[f], Gross, Joachim[c,e], Wolters, Carsten H.[c,e], Sprenger, Andreas[b,g,h] & Lencer, Rebekka[a,b,e,i]

[a] Department of Psychiatry and Psychotherapy, University of Lübeck, 23562 Lübeck, Germany
[b] Center of Brain, Behavior and Metabolism (CBBM), University of Lübeck, 23562 Lübeck, Germany
[c] Institute for Biomagnetism and Biosignalanalysis, University of Münster, 48149 Münster, Germany
[d] Institute for Analysis and Numerics, University of Münster, 48149 Münster, Germany
[e] Otto Creutzfeldt Center for Cognitive and Behavioral Neuroscience, University of Münster, 48149 Münster, Germany
[f] Department of Neurophysiology and Pathophysiology, University Medical Center Hamburg-Eppendorf, 20246 Hamburg, Germany
[g] Department of Neurology, University of Lübeck, 23562 Lübeck, Germany
[h] Institute of Psychology II, University of Lübeck, 23562 Lübeck, Germany
[i] Institute for Translational Psychiatry, University of Münster, 48149 Münster, Germany

[*] Corresponding author at: Department of Psychiatry and Psychotherapy, University of Lübeck, Ratzeburger Allee 160, 23562, Germany; janole.radecke(at)uni-luebeck.de

Declarations of interest: None.

Acknowledgements: This work was supported by the German Research Foundation (DFG; WO1425/10-1 to CHW, GR2024/8-1 to JG and LE1122/7-1 to RL) and by the Bundesministerium für Gesundheit (BMG; ZMI1-2521FSB006, under the frame of ERA PerMed as project ERAPERMED2020-227). JG was further supported by the DFG (GR2024/11-1, GR2024/12-1, TRR393). JOR was funded by the Clinician Scientist program of the Section of Medicine of the University of Lübeck. We thank Dr. Martin Göttlich and Andreas Wollbrink for technical support, Karin Wilken, Hildegard Deitermann, Ute Trompeter, Susanne Schellbach and Mandy-Josephine Reichhardt for support with the data acquisition, and Prof. Peter Trillenberg for helpful discussions.

Personalized tDCS targeting visual motion area V5 modulates smooth pursuit initiation

Abstract

Smooth pursuit eye movements provide an ideal model of sensorimotor integration with visual motion area V5 being a key candidate integrating visual motion processing with oculomotor control. We applied personalized transcranial direct current stimulation (tDCS) explicitly targeting individual V5 to induce subtle impairment or facilitation of sensorimotor integration during pursuit and assess the gain by personalized, compared to conventional normative tDCS. Pursuit initiation was specifically delayed during personalized cathodal tDCS targeting right V5 pointing towards the involvement of specific functional subareas of V5. The results were well-controlled by anodal and sham tDCS, different pursuit tasks, and by two control experiments, one that applied personalized tDCS targeting FEF and another that applied normative tDCS over V5, for all of which no pursuit modulation was observed. Importantly, in contrast to normative tDCS, personalized tDCS effectively modulated pursuit by adapting electric fields to individual anatomical and neurophysiological V5 properties, yielding interesting potential for the improved effectiveness of personalized tDCS in general.

Keywords: non-invasive brain stimulation (NIBS); personalized transcranial electric stimulation (tES); oculomotor; human MT+; sensorimotor transformation; personalized transcranial brain stimulation (TBS); individualized; targeted

Abbreviations: SP: Smooth pursuit eye movements; tES: transcranial electric stimulation; tACS: transcranial alternating current stimulation; tDCS: transcranial direct current stimulation; FEM: finite element method; DWI: diffusion weighted imaging; MRI: magnetic resonance imaging; EEG: electroencephalography; MEG: magnetoencephalography; MEEG: combined EEG and MEG; FEF: frontal eye field; BOLD: blood oxygen level dependent; SMS: simultaneous multislice; TRI: continuous pursuit task; LCMV: linearly-constrained minimum variance; DCMI: distributed constrained maximum intensity; TRIBL: continuous pursuit task with blanking; SR: foveopetal step-ramp task; LMM: linear mixed model; MT: middle temporal visual area; MST: medial superior temporal area;

1. Introduction

Smooth pursuit eye movements (SP), in conjunction with saccades, significantly shape our daily interactions with the environment [1] and provide an ideal model for studying sensorimotor integration mechanisms [2,3]. As part of the neural network underlying eye movement control [4,5], the extrastriate visual motion area V5/MT+ [6] has been identified as a key hub for the integration of visual motion processing during SP [2,7–12].

Based on the temporal evolution of pursuit, sustained SP maintenance is typically dissociated from SP initiation. SP during the initial 100 ms after pursuit onset is mainly driven by bottom-up visual motion information and thus is termed *open-loop* since top-down feedback control is not yet established [2]. In contrast, sustained SP maintenance is generally understood as *closed-loop* controlled due to the reciprocal interactions between bottom-up information about visual motion on the retina and top-down oculomotor feedback signaling [11] including efference copy integration of the oculomotor command and cognitive factors providing predictive and anticipatory input to SP generation and maintenance [13–15]. Animal physiology studies demonstrated that open-loop SP initiation is predicted by activity in the V5-equivalent area MT+ [12,16–18]. Furthermore, lesion studies of MT+ in macaque monkeys demonstrated impaired SP initiation and maintenance [19–22]. This evidence is complemented by microstimulation of MT+ that increased SP velocities towards the stimulated hemisphere (i.e., ipsiversive SP), and decreased contraversive eye velocities [10]. Accordingly, human lesion studies including area V5 have demonstrated both impaired SP initiation and SP maintenance [23–25]. In line with this, suprathreshold neuromodulation by transcranial magnetic stimulation (TMS) targeting right V5 in humans induced an overall decrease of ipsiversive (i.e., rightward) SP velocity [26]. Furthermore, functional imaging studies associated activity in the human area V5 with SP stimulus speed on the one hand as well as the corresponding eye velocity on the other hand, with pronounced V5 activity in the right hemisphere, compared to the left hemisphere [27–29].

Neuromodulation of V5 in the healthy brain by subthreshold stimulation techniques provides an interesting model for a better understanding of the role of V5 for SP [30]. Furthermore, such techniques can be used to mimic subtle functional impairments of sensorimotor integration, observed in the elderly or clinical populations [14,15,31–35]. More specifically, subtle subthreshold neuromodulation by transcranial electric stimulation (tES), including direct current (tDCS) and alternating current stimulation (tACS) can induce transient online-effects and after-effects that outlast the actual stimulation. Several studies induced altered visual motion processing using tDCS or tACS [36–41], but the effect of tDCS on sensorimotor transformation remains elusive. To our knowledge, only one recent study applied normative tDCS over V5 [30] to explicitly modulate sensorimotor integration during SP but did not describe tDCS-induced changes of SP performance.

Conventional tDCS, and tES in general, suffers from a high proportion of non-responders [42–44] and overall small effect sizes in meta-analytic evaluation [45,46]. This may partly be explained by the fact that conventional tDCS uses the identical normative scalp electrode montage across subjects that neglect inter-individual differences. Based on extensive research on finite element method (FEM) simulations of individual transcranial electric fields [47], it has been

shown that volume conduction effects shape individual tES electric fields that vary near the putative effective threshold to induce subthreshold neural modulation [47–50]. Importantly, relations between individually simulated electric fields as the effector of tES and neurophysiological markers of tES effects [51–53] and behavior [54–56] have been described. Based on these challenges of normative tES, it has been suggested to use algorithmic optimization to personalize tES montages, based on explicit assumptions about the individual anatomy and target properties [47,57–59] to control individual transcranial electric fields [60,61]. In the above-mentioned study of Radecke and colleagues [30], for example, no SP modulation by tDCS was described, but FEM simulations of transcranial electric fields indicated low directional intensities for the applied normative montage that were significantly smaller compared to personalized electric field intensities. However, actual experimental applications of personalized tES remain sparse [54,62–64], probably due to the high cost and, consequently, limited examples for the actual gain of personalized compared to normative tES.

In the present study we applied personalized tDCS targeting V5 in the right hemisphere (experiment 1) to specifically modulate V5-associated open-loop SP initiation and closed-loop maintenance of ipsiversive (i.e., rightward) SP (Fig. 1). We tested this hypothesis by explicit definition of the individual target V5 and realistic anatomical head models (structural MRI and diffusion weighted imaging, DWI) to compute personalized tDCS montages and thus individually targeted and algorithmically optimized tDCS electric fields. Functional magnetic resonance imaging (MRI) was employed to estimate individual V5 target location and combined electro- (EEG) and magnetoencephalography (MEG; combined MEEG) to estimate target orientation. We assessed the effect of personalized anodal, cathodal and sham tDCS on different aspects of sensorimotor integration during SP, namely SP initiation, maintenance of continuous SP, and top-down control of SP. We hypothesized antagonistic effects of personalized cathodal versus anodal tDCS targeting V5 on ipsiversive SP initiation and maintenance that builds up during tDCS (online-effects) and outlasts the actual stimulation (after-effects). Furthermore, two control experiments were included to test a) the spatial specificity of tDCS targeting V5 compared to personalized tDCS targeting the right frontal eye field (FEF; experiment 2), and b) the gain by personalized tDCS targeting V5 compared to normative tDCS over V5 (experiment 3).

2. Results

2.1 Personalized tDCS adapts to inter-individual target variability

Individual stimulation targets showed varying location and orientation (Fig. 2A-B). Specific SP-related BOLD activity was observed in individually estimated V5 locations near previously reported V5 coordinates (x/y/z MNI-coordinates, V5: 45/-67/2 ± 3/6/4; Tab. S1) [7,65]. Individual V5 activation maxima deviated by 7 ± 3 mm Euclidean distance to the mean location, yielding a considerable inter-individual variability of tDCS target locations (Fig. 2B). Second-level analysis of BOLD activity revealed a significant increase of V5 activity during continuous pursuit, compared to fixation in a cluster in inferior and middle occipital, as well as middle and inferior temporal cortex of the right hemisphere (cluster size k = 97, cluster p = .007, local maximum: 42/-73/2, t_{18} = 7.6) [66]. For illustration, individual statistical maps from the Pursuit

versus Fixation contrast were interpolated on the MNI brain, and FDR-corrected one-sample *t*-tests are shown (Fig. 2A). In addition, the correct estimation of individual V5, was confirmed by small volume analyses using a 10 mm radius centered around the mean coordinate of individually estimated V5 local maxima comparing BOLD activity during continuous SP compared to fixation (Fig. 2A; Tab. S1; t_{18} = 6.7, p < .001). A mask of the V5-equivalent cytoarchitectonic area hOc5 was additionally applied and confirmed a significantly increased BOLD activity in V5 during SP compared to fixation (t_{18} = 6.3, p < .001, center coordinates: 45/-61/2) [6]. In line with the heterogenous cortical structural organization of V5, the estimated stimulation target orientations showed a variety of quasi-radial, and quasi-tangential orientations across participants (Fig. 2B).

Personalized tDCS montages targeting individual right V5 confirmed a clear adaptation to the target location and orientation, placing cathodes on the scalp roughly over the target in the direction of estimated target orientation. Across subjects, exemplary for the application of personalized cathodal tDCS, a cluster of anodes was observed including electrode positions P6, P8, and CP6, whereas a cluster of cathodes was observed including electrode positions PO8, PO10, O2, and O10. However distinct target orientations and quasi-radial target orientations are reflected by varying tDCS electrode positions across the scalp (Fig. 2C) [61]. Overall SP performance was high in the expected range for young healthy participants (Tab. 2, see Supplement) [30].

2.2 Personalized tDCS targeting V5 specifically modulates pursuit initiation

Personalized tDCS targeting V5 was applied to modulate SP performance depending on tDCS condition (sham, anodal, cathodal), timepoint (t_0, t_{TDCS_5}, t_{TDCS_10}, t_{TDCS_15}, t_{TDCS_20}, t_{15}, t_{40}) and SP stimulus direction (leftward, rightward). Personalized tDCS targeting V5 specifically modulated SP latencies in the SR task, as revealed by an omnibus analysis (three-way interaction: p = .044; Fig. 3A-C, Tab. S2). Additional LMM analyses indicated an online effect during tDCS (p = .015; Fig. 3A-C, Tab. 3), but no tDCS after-effects (p = .484; Tab. 4). Specifically personalized cathodal tDCS delayed rightward SP latencies for t_{TDCS_20}, relative to t_{TDCS_5} (p = .002, d_z = 0.93). A follow-up analysis confirmed that overall SP latencies across all timepoints of the sham session (t_0, t_{TDCS_5} to t_{TDCS_20}, t_{15}, t_{40}) were delayed for leftwards compared to rightwards SP (p = .007, d_z = 0.64; compare Fig. 3A), indicating that personalized cathodal tDCS targeting the right V5 hampered latencies of rightward SP to the level of initially delayed leftward SP latencies. In addition, a paradoxical effect by personalized cathodal tDCS was observed during t_{TDCS_15} between leftward and rightward SP latencies (p = .002, d_z = 0.89) and latencies for leftward SP during t_{TDCS_15} were significantly delayed for personalized cathodal tDCS, compared to sham (p = .042, d_z = .72; Fig. 3A).

To follow-up tDCS online effects for rightward SP latencies (Fig. 3A), these were defined both as difference between the first and last timepoint during t_{TDCS} ($t_{TDCS_20} - t_{TDCS_5}$; 18 [12, 29] ms, bootstrapped mean and [95%-confidence interval]; Fig. 3B), as well as the slope of a linear fit across all four t_{TDCS} timepoints (t_{TDCS_5} to t_{TDCS_20}; 4.9 [2.8, 8.3] ms/5 minutes ; Fig. 3C). While the difference tDCS effect can be directly related to the significant post-hoc contrasts of the LMM analysis, the slope tDCS effect yields a more robust estimate considering the paradoxical

effect, but thereby introduces potential noise from the SP latencies observed during t_{TDCS_10} and t_{TDCS_15}. Therefore, we consider the difference and slope estimates of the tDCS effect as complementary. Significant differences between personalized anodal and cathodal tDCS for the rightward SP latencies were revealed for both difference (z = -3, p = .008, d_z = 0.72) and slope estimates (z = -2.58, p = .03, d_z = 0.61) of tDCS effects. In addition, difference tDCS effects differed between leftwards and rightwards SP latencies during personalized cathodal tDCS (z = -2.41, p = .024, d_z = 0.59). The corresponding effect for the slope estimate did not survive Bonferroni-correction (p = .11). In addition, the difference tDCS effect was significantly larger for personalized cathodal tDCS targeting V5, when compared to personalized tDCS targeting FEF (z = 2.08, p = .019, d_z = 0.5) while the same effect for the slope estimate missed significance (p = .057).

During tDCS, an online effect on initial acceleration was also observed (p = .02; Tab. 3), however, this effect was not indicated by the preceding omnibus analysis and post-hoc tests did not survive correction for multiple comparisons.

Besides the modulation of SP latencies, no specific tDCS effects (i.e., tDCS condition * timepoint or tDCS condition * timepoint * direction interaction effects) were observed for tasks indicating sustained SP maintenance performance with continuously visible targets (TRI), top-down mechanisms involved in ongoing SP with temporary target blanking (TRIBL) or closed-loop SP performance during the SR task following open-loop initiation (all p > .523; Tab. 3-4, Tab. S2). Furthermore, neither personalized tDCS targeting the right FEF as a control region (within-group, p = .862; Fig. 3D-F, Tab. S4), nor normative tDCS over V5 (p = .93; between-group, matched sample of N = 19; Fig. 3G-I, Tab. S5) induced a modulation of SP latencies during tDCS comparable to the observed effects for personalized tDCS targeting V5 (Fig. 3A-C). Finally, the results were not compromised by individual tDCS side-effects (see Supplement).

2.3 Personalized tDCS targeting V5 affects simulated transcranial electric fields and increases tDCS effect, compared to normative tDCS over V5

To evaluate the electric field differences presumably leading to distinct tDCS effects, electric field simulations were compared between the applied personalized tDCS targeting V5 and the normative V5 montage for N = 19 subjects from experiment 1 (personalized V5; Fig. 2C-F). Electric field simulations showed comparable target intensities (p = .209, normative $|E|_{IT}$ = 0.62 ± 0.38 V/m, personalized $|E|_{IT}$ = 0.66 ± 0.45 V/m, M ± SD). However, normative electric fields across the cortex showed significantly increased intensities in non-target dorsal and medial parts of bilateral parietal cortex compared to personalized electric fields. In contrast, personalized electric fields showed increased intensities in the right lateral occipital-parietal-temporal cortex compared to the normative electric fields (Fig. 2F). In addition, directionalities were significantly increased for personalized compared to normative electric fields (z = -4.87, p < .001, d_z = 1.11; normative $|E|_{DIR}$ = 0.05 ± 0.32 V/m, personalized $|E|_{DIR}$ = 0.42 ± 0.28 V/m, M ± SD; Fig. 2F). Electric field spatial extent was significantly decreased for personalized, compared to normative tDCS (z = 6.81, p < .001, d_z = 1.74 normative $|E|_{EXTENT}$ = 70 ± 2 mm, personalized $|E|_{EXTENT}$ = 57 ± 8 mm, M ± SD; Fig. 2F). In conclusion, personalized electric field

topographies were shifted towards individual tDCS targets in the right V5, thus effectively considering the varying individual tDCS target locations and orientations in the right V5 and reducing co-stimulation of non-target parietal cortex, compared to the normative electric fields.

Indeed, the evaluation of tDCS effects on ipsiversive SP latencies revealed significantly increased tDCS effects for personalized cathodal tDCS targeting V5 compared to normative tDCS over V5 (difference tDCS effect: $z = 2.1$, $p = .018$, $d_s = 0.7$; slope tDCS effect: $z = 1.81$, $p = .036$, $d_s = 0.61$).

3. Discussion

We conducted a comprehensively controlled experiment to assess the effects of personalized tDCS targeting V5 on SP initiation and maintenance as a direct behavioral read-out of tDCS effects on sensorimotor integration. We found a spatially and functionally specific, significant modulation of SP initiation by personalized cathodal tDCS (sections 3.1 and 3.2) that was absent during anodal or sham tDCS. This effect was independent from possible practice effects [30] and tDCS side-effects (Supplement). Furthermore, electric field simulations and a control experiment applying normative tDCS over V5 signify more precise electric fields and an increased gain by personalized tDCS in contrast to normative tDCS (section 3.3).

3.1 Personalized tDCS targeting V5 specifically modulates open-loop pursuit initiation

To interpret our key finding of specific SP initiation modulation (i.e., SP latencies) by personalized cathodal tDCS, it is important to consider the multimodal role of the human visual area V5/MT+. As laid out in the introduction, this area can be functionally dissociated into the middle temporal visual area (MT) and the medial superior temporal area (MST) [7,9]. In the macaque monkey, it has been shown that MT receives bottom-up visual information [67,68] and integrates these to signal visual motion on the retina as a velocity signal during SP [11]. MST receives projections from MT [68] and MST itself maintains reciprocal connections to various visual areas, as well as parietal and premotor nodes of the oculomotor network [67,69]. It has been proposed that these connections to MST govern top-down signals during ongoing SP coding, e.g., predicted target motion even in the absence of a visual target [11]. Importantly, neural activity in MT+ is involved in SP initiation, but relies on gain control by higher-order network nodes such as the FEF [12,16,18]. In line with these studies, human V5/MT+, comprising putative MT and MST, has been suggested as a key hub for the sensorimotor transformation during SP [7,70], thus integrating bottom-up visual motion information with top-down oculomotor control during open-loop SP initiation and closed-loop SP maintenance.

In the present study, open-loop SP initiation (SP latency, SR task) was hampered by personalized cathodal tDCS targeting V5. The observed impairment of ipsiversive, but not contraversive, SP is in line with previous TMS modulation of the right V5 in humans [26]. Animal studies described an impairment of ipsiversive SP for foveopetal step-ramps after lesions of the foveal representation of MT [20,22]. Human lesion studies including V5 described similar ipsiversive SP deficits [23–25]. However, the same authors also differentiate contralesional SP deficits (retinotopic) from directional deficits that affect SP ipsiversive to the lesion site [20,23–

[25]. During the step of the applied SR task, the visual target is moved 2.5 ° to one side, before it starts to move in the opposite direction with a constant velocity ramp. This paradigm allows subjects to start pursuit without an initial saccade as soon as the visual target crosses the point of the subjects' central fixation at the start of each trial. However, this also implies that in the time between the step onset and the midline-crossing of the visual target, subjects fixate the center of the screen and thus are presented a retinotopic visual stimulus moving from the step eccentricity towards the participant's central fixation, before the visual target is then fixated during the actual pursuit. In the present experiment personalized cathodal tDCS presumably induced retinotopic deficits that affected sensorimotor transformation after the leftward target step onset moved the visual target to the hemifield contralateral to the targeted right V5, but before the onset of rightward SP. This would explain the observed isolated deterioration of SP latencies that might follow retinotopic deficits in the hemifield contralateral to the targeted right V5. At the same time initial acceleration (SR task), SP maintenance (TRI task) and top-down aspects of SP in the blanking task (TRIBL task) remained unaffected which would rather indicate directional effects [21]. Retinotopic SP deficits could indicate the involvement of peripheral representations in MT, in contrast to foveal MT representations, and/or adjacent MST parts. Lesions of the latter also result in directional SP deficits [19,20,22]. In contrast to tDCS targeting V5, no SP modulation was observed by tDCS targeting right FEF, further marking the spatial specificity of personalized tDCS targeting right V5. Taken together, we conclude that in our experiment personalized cathodal tDCS specifically modulated early open-loop sensorimotor transformation within V5 putative subregion MT, or feedforward communication from MT to MST. We further speculate, either that foveated sensorimotor transformation was not affected by personalized cathodal tDCS, or that tDCS-induced initial open-loop directional disturbances were compensated by higher-order cognitive mechanisms coming into play under closed-loop control of SP [13–15,71,72].

3.2 Personalized cathodal tDCS targeting V5 transiently reduces cortical excitability

Conventionally, cathodal tDCS has been defined as placing the cathode over the assumed target region to reduce cortical excitability (and increase excitability by anodal tDCS) [73]. Among other mechanistic explanations for tDCS [74], it has been proposed that tDCS electric fields induce cortical membrane polarizations that lead to a subthreshold modulation of neuronal firing-rates and altered cortical excitability [73,75], in addition to changes of blood flow [76] and local GABA/glutamate metabolism at the stimulation site [77–79]. Cathodal tDCS specifically was described to reduce cortical excitability [73,75] and local glutamate concentration [78]. Therefore, personalized cathodal tDCS in the present study presumably reduced cortical excitability in V5, thereby hampering the integration of visual motion information to elicit SP initiation as indicated by delayed SP latencies.

We observed a transient modulation of SP latencies by single-bout personalized cathodal tDCS (online-effect). No after-effects were observed 15 minutes after tDCS or thereafter. A more detailed analysis of the temporal evolution of SP initiation over the 20 minutes tDCS showed that this online effect evolved slowly resulting in a significant latency difference between the first (t_{TDCS_5}) and the last (t_{TDCS_20}) read-out timepoints. Immediate tDCS modulations were

328 previously shown to induce NMDA-receptor mediated long-term plasticity (LTP) or long-term
329 depression (LTD) that drive longer-lasting tDCS effects [80–82]. Thus, we conclude that
330 personalized cathodal tDCS in the present study induced immediate changes in MT excitability
331 which exerted a statistically robust tDCS effect on behavioral SP performance only when tDCS-
332 induced LTD-like effects were established after several minutes of continuous tDCS.
333 In previous studies, both anodal and cathodal tDCS over V5 induced an improvement in the
334 discrimination accuracy of coherent motion perception in visual scenes [41]. Following previous
335 speculations [38], Battaglini and colleagues [41] suggested that, on the one hand, anodal tDCS
336 increases coherent motion discrimination by increasing the excitability of neurons in the
337 putative subregion MT of V5 that are tuned to correlated motion signals. On the other hand,
338 cathodal tDCS reduces the overall excitability of MT, thereby relatively reducing the response
339 to uncorrelated noise in competing motion scenes with low coherence. At the same time,
340 cathodal tDCS also reduces the discrimination of coherent motion signals in situations with
341 high signal-to-noise ratio. In line with this evidence, we observed a specific impairment of the
342 direct and naturalistic SP sensorimotor response to a single moving visual target without
343 competing motion noise (i.e., with high signal-to-noise ratio) during personalized cathodal
344 tDCS. We further speculate that we did not observe performance facilitation by personalized
345 anodal tDCS in the present young, healthy participants due to a ceiling effect [83] of their anyway
346 high SP performance, in addition to practice-associated improvements obtained during the
347 study (Supplement) [30]. In contrast to this, impaired SP latencies observed in the elderly and
348 clinical populations [14,15,31], might be improved by anodal tDCS representing interesting target
349 populations to further examine the clinical benefits of (personalized) tDCS for future studies.
350 Taken together, by applying personalized, i.e., targeted tDCS and differentiating distinct
351 functional properties of SP, we can pinpoint the modulation of SP latencies by personalized
352 cathodal tDCS to an early phase of sensorimotor transformation, presumably involving
353 reduced excitability and LTD-like modulation of V5 subregion MT which delays SP
354 performance.
355
356 **3.3 Normative tDCS over V5 does not modulate pursuit initiation**
357 In contrast to the specific modulation of ipsiversive SP latencies during personalized tDCS
358 targeting V5, no online effect was observed by normative tDCS over V5, extending the findings
359 of our previous study [30]. Previously we showed that normative tDCS over V5 did not result in
360 any tDCS after-effects on SP [30]. However, simulations of tDCS electric fields in a small sample
361 (N = 6) already suggested rather small target directionalities by normative tDCS that could be
362 increased by personalized tDCS montages with respect to individual targets. Here, we confirm,
363 in a much larger sample, that normative tDCS over V5 yields limited target directionalities,
364 compared to personalized tDCS targeting V5. This improvement of simulated personalized
365 compared to normative electric fields is in line with previous findings of increased
366 personalized directionalities when targeting the parietal cortex [61], the somatosensory cortex
367 [62] and increased electric fields across the brain and within the target region for personalized
368 electric fields targeting the auditory cortex [64]. Furthermore, we extent previous findings by
369 whole-brain analysis of personalized compared to normative simulated electric fields

370 indicating reduced spatial extent of the targeted electric fields and a shift of the electric field
371 topography away from bilateral parietal regions and towards individual target V5 estimates in
372 temporal regions within the right hemisphere (Fig. 2E-F). In contrast, normative electric fields
373 showed significantly increased intensities in non-target dorsal and medial parts of bilateral
374 parietal cortex compared to personalized electric fields.
375 Although it has been proposed repeatedly to implement electric field simulations and
376 optimization in tES protocols [49,57–59,84], actual applications of personalized tES remain rare [54,62–
377 64]. Thus, little is known about the gain of personalized, compared to conventional normative
378 tES. Therefore, in addition to the analysis of simulated electric fields, we investigated whether
379 the observed behavioral online effect of personalized cathodal tDCS on ipsiversive SP latencies
380 were specific to the applied personalization approach, by re-analyzing data from a matched
381 sample where normative tDCS was applied over the right V5. In contrast to personalized tDCS
382 targeting V5, we did not observe a modulation of SP during normative tDCS over V5. A more
383 detailed analysis indicated a significantly increased tDCS effect on SP by personalized cathodal
384 tDCS, compared to normative cathodal tDCS. We thus follow that the increased efficacy of
385 personalized compared to normative tDCS targeting/over V5 as indicated by electric field
386 simulations holds true for the modulation of SP latencies. Only a few previous studies provided
387 data from applied personalized tDCS [62] or tACS [54,63,64] and only two of those provided a direct
388 comparison of personalized versus normative tES [62,64]. To our knowledge, as of now, no study
389 described the gain by personalized compared to normative tDCS with respect to the
390 modulation of behavior. Khan and colleagues [62] found a significant modulation of the M20
391 somatosensory evoked component by personalized tDCS targeting the underlying dipolar
392 source in Brodmann area 3b in N = 10 subjects, but no effect by normative tDCS. In the same
393 study, personalized transcranial electric fields optimized with the DCMI algorithm [85] reached
394 simulated target directionalities of 0.38 ± 0.21 V/m, compared to 0.26 ± 0.13 V/m for
395 normative tDCS with 2 mA current applied on the scalp. In line with these results, our present
396 data indicate that personalized tDCS using the DCMI algorithm shifts the electric field
397 topography towards the explicitly defined tDCS target and thereby increases target
398 directionalities above the effective threshold at the group-level. Normative tDCS may not
399 produce reliable results, due to the relatively limited and untargeted electric fields. Here, we
400 present data that indicates the gain by personalized compared to normative tDCS with respect
401 to SP performance as direct behavioral read-out of the tDCS-effect. Especially in the light of a
402 growing interest in tDCS for clinical application [86,87], our present findings support the huge
403 potential of personalized tES approaches directing individual transcranial electric fields to the
404 assumed cortical target thereby maximizing the individual stimulation effect.
405 In another study, the application of 2 Hz tACS targeting the auditory cortex (stimulation
406 intensity: ±0.5 mA) induced a phase-specific modulation of frequency-modulated sounds by
407 personalized tACS, but the same effect was described for normative tACS [64]. In this light, it
408 must be noted that personalized tES does not necessarily increase effectiveness, compared to
409 normative tES. Indeed, normative tES can greatly reduce the resources required for
410 experimental and clinical application considering additional data acquisition and analysis for
411 target localization, individual head models, and electrode positions needed for the

optimization and careful application of personalized tES [49]. To conclude, we suggest that personalized and normative approaches should be handled complementary: By specific assumptions about the individual anatomy and the individual functional tES targets, personalized tES is predestined to test hypotheses about the functional mechanisms underlying specific tES applications, for example the role of V5 in the modulation of SP, as shown in the present study. Naturally, personalized tES combines the analysis of tES read-out parameters with simulated electric fields and neurophysiological data that can inform and extend the analysis. These insights can then be used to validate implicit assumptions of normative tES applications or to *a priori* inform the optimization of next-generation, resource-efficient and effective normative tES montages, as a complementary approach to data-intensive *a posteriori* optimization of normative tES montages [56,88].

4. Conclusion

In this study, tDCS was applied to modulate sensorimotor integration during SP. Our main finding shows that personalized cathodal tDCS targeting right V5 specifically delayed latencies of ipsiversive SP. Taking together the analysis of functional aspects of SP, electric field simulations, and previous literature, we conclude that tDCS in the present study modulated either early sensorimotor transformation in the V5 functional subarea MT or feedforward communication between MT and MST. The results were extensively controlled by functional assessment of different SP aspects, anodal and sham tDCS, by application of personalized tDCS over FEF as a spatial control region, and normative tDCS applied over V5, for all of which no SP modulation was observed. Especially FEM simulations of electric fields suggest that the gain of (effective) personalized tDCS, compared to (ineffective) normative tDCS can be attributed to topographical shifts of personalized transcranial electric fields towards the targeted right V5 at group-level, as well as increased target directionalities and reduced spatial extent. These results yield an interesting methodological perspective for the translation of effective tDCS, and tES in general, to clinical research and therapeutical settings.

5. Materials and methods

5.1 Participants and procedure

Twenty healthy participants were recruited to apply personalized tDCS targeting V5 (experiment 1) and FEF (experiment 2), respectively. One participant did not proceed the experiment after the first experimental session due to personal reasons. Thus, complete datasets of N = 19 participants were included in the analyses (Tab. 1). To compare results from personalized tDCS to the application of normative tDCS, a subsample from a previous study applying normative tDCS over V5 [30] was statistically matched to the personalized tDCS sample with respect to age, gender, laterality index, MWT-B percentile ranks and BDI-II raw values (paired *t*-tests, all $p \geq .25$; Tab. 1). All participants reported no history of psychiatric or neurological disorders and no psychotic disorders of first-degree family members. Participants had normal or corrected-to-normal visual acuity (1 ± 0.1) and gave written informed consent in line with the declaration of Helsinki prior to the experiment. The study was approved by the ethics committees of the Universities of Lübeck and Münster (#20-459 and #2015-263-f-S).

In a full within-subject design, participants completed a battery of SP tasks during eight experimental sessions (Fig. 1). During the first session, structural MRI data was recorded to compute individual FEM head models. Additionally, fMRI activity was recorded while subjects performed a SP task to localize areas V5 and FEF, in each participant individually. During the second session, combined MEEG was recorded while SP was performed to define the target neuronal orientation at the fMRI-based locations of V5 and FEF [89]. In addition, MEEG data was recorded during electrical stimulation of the median nerve to estimate individual skull conductivities based on somatosensory evoked MEEG activity (Antonakakis et al., 2020; Schrader et al., 2020) to enable combined MEEG source analysis and target orientation determination. In the following sections, we describe how we used the resulting individually skull-conductivity calibrated FEM head models (section 5.2) to compute personalized tDCS montages for the individual targets in V5 and FEF (section 5.3 and 5.4). Subsequently, sham-controlled personalized anodal and cathodal tDCS targeting areas V5 and FEF was applied in six subsequent experimental sessions (section 5.5) to modulate SP performance (section 5.6). In addition, personalized tDCS targeting V5 was compared to normative V5 over V5, with respect to simulated transcranial electric fields and SP performance under modulation by tDCS (section 5.7). In section 5.8 the statistical analysis is described.

5.2 Calibrated individual FEM head models

Structural MRI data were recorded using a 3-T Siemens Magnetom Skyra scanner (Siemens, Germany) and a 64-channel head coil. In addition to T1- and T2-weighted images (T1: 3D MP-RAGE sequence, TR = 2300 ms, TE =3.6 ms, TI = 1100 ms, FA= 8°; T2: spin echo pulse sequence, TR = 3200 ms; TE = 408 ms, FA = 120°; both at 1 x 1 x 1 mm resolution and 192 x 256 x 256 mm FoV), DWI data were acquired for 64 direction vectors (turbo spin echo sequence, 69 volumes, 1 x 1 x 1 mm resolution, 100 x 100 x 72 mm FoV, SMS with slice acceleration factor 4, TR = 5500 ms, TE = 128 ms, FA = 90°, b = 1000 s/mm^2) and five additional volumes were acquired with diffusion sensitivity b = 0 s/mm^2.

Individual geometry-adapted six-compartment hexahedral FEM head models were computed, including calibrated skull conductivities and white matter conductivity anisotropy [30,90] with the DUNEuro toolbox [i] (see Supplement for details). Conductivities were set to normative values for scalp (0.43 S/m), CSF (1.79 S/m), gray matter (0.33 S/m) and white matter (0.14 S/m). For the EEG lead field, skull conductivities were individually calibrated (skull compacta: 0.013 ± 0.01 S/m, skull spongiosa: 0.0468 ± 0.036 S/m; see Supplement) [90,91]. Finally, the EEG lead fields for estimation of the tDCS target orientations, and individual geometry matrices for the tDCS optimization were computed using the calibrated skull conductivities.

5.3 Functional localization of V5 and FEF tDCS targets

Personalized tDCS montages were computed based on individual estimates of the stimulation targets in areas V5 (experiment 1) and FEF (experiment 2) of the right hemisphere, respectively (Fig. 1E, Fig. 2) [30], as described in more detail below.

[i] https://www.medizin.uni-muenster.de/duneuro/startseite.html

First, to determine the target locations of V5 and FEF using fMRI, blood oxygen level dependent (BOLD) activity was recorded (simultaneous multislice (SMS) with acceleration factor 4, 307 Volumes, TR = 980 ms, TE = 30 ms, FA = 70°, resolution 3 x 3 x 3 mm, 68 x 68 x 56 mm) while participants performed SP (red dot as SP target, diameter 0.5°, black background; 1920 x 1080 screen resolution, 60 Hz refresh rate, NordicNeuroLab, Norway) and eye movements were recorded (Eyelink 1000Plus, 1000 Hz sampling rate; SR Research Ltd., Canada). Participants completed a test battery of SP-tasks similar to the tasks during the tDCS experiments (see Supplement). Each pursuit block was preceded by fixation intervals with a centrally presented red dot (12 s, diameter 0.5°). Functional images were slice-timing corrected, smoothed (6 mm FWHM Gaussian kernel), and co-registered to the normalized T1 image. Individual locations of visual area V5 and FEF in the right hemisphere were determined as local maxima of BOLD activity during SP near putative V5 and FEF regions (Tab. S1) [7,65] in contrast to fixation intervals (*t*-test, $p < .05$ across 5 adjacent voxels, FWE-corrected).

Second, individual target orientations were estimated using beamforming at the right V5 and FEF target locations defined by functional MRI. Therefore, combined MEEG data were recorded (EEG: 60 channels, Easycap, Germany; MEG: 275 axial gradiometers, VSM MedTech Ltd., Canada; 600 Hz sampling rate) while participants completed a continuous pursuit task (TRI; 18.7°/s, ±15° amplitude, 20 blocks of each 8 ramps to the left and right interleaved with short breaks). Before the first block and after the 10th block, participants fixated a red dot in the center of the screen for 15 s. Data were filtered (0.1 Hz highpass-filter, 50 Hz notch filter considering harmonics), cut into 320 epochs (0 to 1.59 s length relative to ramp onsets to left and right), and demeaned. Invalid epochs were rejected semi-automatically (rejected trials: 15.3 ± 11.3 %) and the EEG data was re-referenced to the average reference. tDCS target orientations were estimated using linearly constrained minimum variance (LCMV) beamforming with Unit-Noise-Gain constraint (regularization parameter $\lambda = 5\%$), following the procedure described in [89] (see Supplement for details).

Electrode positions for the tDCS montage optimization were recorded (FASTRAK, Polhemus Inc., VT/USA). These 74 electrode positions follow the 10-20-system, embedded in a standard EEG cap layout (Easycap, Germany), of which 60 electrodes were used as EEG sensors.

5.4 Computation of personalized tDCS montages and electric field simulations

Based on individual anatomical information, integrated in the head models (section 5.2) and individual target information from the localizer tasks (section 5.3), personalized tDCS montages were computed to optimally target the area V5 (experiment 1) or FEF (experiment 2), respectively. To this end, the distributed constrained maximum intensity (DCMI) algorithm [54,61,62,85] was employed to compute the personalized tDCS montage that maximizes the injected current at the target location along the target orientation (i.e., the directionality; see Supplement for details). Resulting montages described personalized cathodal tDCS montages. Herein, we define the applied personalized tDCS montages relative to the estimated target orientations, i.e., personalized cathodal tDCS results in montages with the cathodes placed on the scalp roughly in the direction of the estimated target orientation. For personalized anodal

535 tDCS, the polarity of each electrode was inverted. This definition does not resemble normative
536 tDCS conventions where the cathodes/anodes are placed on the scalp directly over the
537 proposed target location defining cathodal/anodal tDCS. This convention implicitly assumes
538 quasi-radial targets but does not consider tangential targets or inter-individual target
539 localization variability. The target orientations in the present study were estimated as the
540 MEEG summed dipole orientation that might not reflect the local cortical structure, but rather
541 functional properties of the target orientation. Therefore, the definition of personalized
542 cathodal/anodal tDCS considers individual target locations and orientations.
543
544 **5.5 Application of personalized tDCS**
545 During tDCS (t_{TDCS}) Personalized anodal, cathodal, or sham tDCS was applied targeting the right
546 V5 and FEF in six pseudo-randomized sessions, separated by at least four days (7.9 ± 7.8 days,
547 M ± SD; Fig. 1C). During each session, 20 minutes of tDCS was applied using a Starstim 8 device
548 (Neuroelectrics, Spain). Small Ag/AgCl electrodes (NG Pistim, 3.14 cm^2 surface) were placed in
549 custom empty EEG caps (EasyCap, Germany) with the same layout and cap size as used for the
550 EEG measurement and electrode registration (section 5.3) to ensure an accurate placement
551 of the stimulation electrodes according to the optimized personalized montages (Fig. 1E;
552 section 5.4). During personalized anodal and cathodal tDCS, a total of 2 mA current was
553 applied (10 s ramp-on and ramp-off). Sham tDCS was applied by the same montages as used
554 for anodal stimulation, but tDCS was applied for only 30 s in addition to the current ramps.
555 To minimize transcutaneous side-effects, anesthetic creme (2.5 % lidocaine, 2.5 % prilocaine,
556 Anesderm®, Pierre Fabre, Germany) was used [92]. After each t_{TDCS} interval, participants
557 completed a questionnaire asking for their subjectively perceived transcutaneous side-effects
558 during t_{TDCS} (itching, warmth, stitching, throbbing, and pain) on a five-point scale (0 = absent,
559 weak, moderate, pronounced, 4 = intense) [93]. Furthermore, participants rated subjective
560 fatigue for four timepoints during t_{TDCS} on a five-point scale (1 = very alert, awake, moderate,
561 tired, 5 = very tired).
562
563 **5.6 Eye tracking and analysis of eye movement data**
564 During the six tDCS sessions, participants were seated 65 cm in front of an LCD monitor in a
565 closed room with lights off and completed three SP tasks to assess different aspects of SP
566 initiation and maintenance [30]. Details on the experimental setup, preprocessing, and analysis
567 of eye movement data are described in the Supplement [30]. In short, eye movements were
568 recorded using a video-based eye tracker (Eyelink 1000Plus, SR Research Ltd., Canada). During
569 all tasks, participants were instructed to follow a horizontally moving SP target on the monitor
570 as precisely as possible (red dot with 0.5° diameter, black background; Fig. 1B). During the first
571 task, eight horizontal constant velocity ramps were presented as continuous triangular
572 waveform stimulus (TRI, 18.7°/s, ± 15° amplitude; Fig. 1B-C, Supplement). In the second task,
573 12 similar horizontal velocity ramps were presented with target blanking between 300 to 1000
574 ms relative to ramp onset (18.7°/s, ± 15° amplitude, triangular waveform stimulus with
575 blanking, TRIBL; Fig. 1B-C, Supplement). To specifically assess SP initiation and early SP
576 maintenance eight horizontal foveopetal step-ramp stimuli (SR) were presented [94], pseudo-

randomly directed either to the left or the right side of the screen. Step-ramps started with a 2.5° step which was immediately followed by a velocity ramp in the opposite direction (18.7°/s, ± 15° amplitude; Fig. 1B-D). To minimize expectation effects, two of eight step-ramps were presented with alternating velocities (9.7 °/s, ± 1.3 ° step-size; 26.7 °/s, ± 3.5 ° step-size). The three tasks were presented in mixed blocks [34] including three task repetitions during each block. This resulted in 24 continuous ramps (TRI), 36 ramps with blanking (TRIBL) and 24 step-ramps (SR) per block.

Effects of tDCS on SP were assessed by presenting each one block of SP tasks before (t_0), and 15 and 40 minutes after (t_{15}, t_{40}; after-effects) tDCS application in each of the six experimental sessions. Online effects of tDCS were assessed by presenting four repetitions of SP task blocks equally distributed across the 20 minutes tDCS application (t_{TDCS}; i.e., within the first 5, 10, 15, or 20 minutes of tDCS, t_{TDCS_5}, t_{TDCS_10}, t_{TDCS_15}, t_{TDCS_20}; Fig. 1C). During t_{TDCS}, SP task blocks were separated by simple oculomotor tasks to activate the oculomotor system during the stimulation, while providing an active rest for the participants at the same time (see Supplement). Overall, this resulted in overall 504 continuous ramps (TRI), 756 ramps with blanking (TRIBL) and 504 step-ramps (SR) that were analyzed for each subject during experiment 1 (V5) and experiment 2 (FEF), respectively.

SP data analysis focused on SP velocity, computed as the first derivative of eye position. Continuous data were epoched (-100 to 1600 ms for TRI and TRIBL relative to the left or right ramp onset and -100 to 1300 ms for SR relative to the ramp onset) and invalid epochs were rejected (experiment 1 (V5): 1.5 ± 2.1 % epochs were rejected). Median eye velocity across epochs was computed separately for each subject, tDCS condition (anodal, cathodal, sham), timepoint (t_0, t_{TDCS_5}, t_{TDCS_10}, t_{TDCS_15}, t_{TDCS_20}, t_{15}, t_{40}) and stimulus direction (leftward, rightward). SP velocity parameters were computed to assess different aspects of SP performance during open-loop SP initiation (SR: SP latency, initial eye acceleration; Fig. 1D) as well as ongoing, i.e., closed-loop SP (SR: early maintenance gain; TRI: maintenance gain, gain = eye velocity/target velocity; TRIBL: preblank, residual and postblank velocity gains, deceleration and deceleration latency at the start of the blanking interval, as well as re-acceleration and re-acceleration latency at the end of the blanking interval) [13,30].

5.7 Comparing personalized tDCS targeting V5 and normative tDCS over V5

Results from personalized tDCS targeting V5 (experiment 1) were compared to results from the application of normative tDCS over V5 (experiment 3; Tab. 1). The normative application of V5 was designed identically to the personalized procedure with respect to the SP test battery and the overall application of tDCS [30] and data from experiment 3 was re-analyzed according to the analysis procedure in experiment 1. However, instead of personalized tDCS montages, normative tDCS montages were used in experiment 3 that did not vary across subjects, thus also no MEEG and MRI data were acquired before the normative tDCS experiment. In short, to apply normative tDCS, two stimulation electrodes were placed over area V5 of the right hemisphere (PO8, P8) with two central return electrodes (Cp1, Cz) [37,38] according to the 10-20 system. During normative tDCS, 2 mA current was applied for 20 minutes, restricted to 1 mA per electrode. Eye movements were recorded during the same

timepoints as in the personalized experiment (t_0, t_{TDCS_5}, t_{TDCS_10}, t_{TDCS_15}, t_{TDCS_20}, t_{15}, t_{40}). Since SP during t_{TDCS} were not analyzed in detail by Radecke et al. [30], the data from the matched sample were re-analyzed for all tDCS timepoints (t_{TDCS_5}, t_{TDCS_10}, t_{TDCS_15}, t_{TDCS_20}) to compare online effects on the SP performance by normative versus personalized tDCS.

Furthermore, electric field simulations were compared between normative and personalized montages to estimate the differences in the potential efficacy between the two tDCS methods, given the individual estimates of the V5 tDCS target. Therefore, normative electric field simulations were computed for the N = 19 subjects from the personalized tDCS sample, using the normative electrode placement, since data for these participants for computation of individual head models and estimation of individual tDCS targets were available. To quantify individual transcranial electric field parameters (see Supplement for details), for each subject, we computed the target intensity ($|E|_{IT}$) the target intensity corrected for the parallelity between the stimulation target orientation vector and the target electric field orientation vector (directionality, $|E|_{DIR}$) [54,61,62], as well as the spatial extent of the electric field relative to the stimulation target ($|E|_{EXTENT}$) [54,61]. The overall cortical electric field ($|\mathbf{E}|$) and electric field parameters with respect to the individual stimulation targets ($|E|_{IT}$, $|E|_{DIR}$, $|E|_{EXTENT}$) were compared between personalized versus normative tDCS. For illustration, individual electric fields were interpolated on a common MNI cortical grid and averaged across subjects (Fig. 2).

5.8 Statistical analysis of tDCS effects

To analyze tDCS effects on SP performance, linear mixed models (LMMs) were fitted to the data (IBM SPSS Statistics, IBM Corp., USA) for each estimated SP parameter and separately for experiment 1 (V5-personalized), experiment 2 (FEF-personalized), and experiment 3 (V5-normative). In a full within-subject design, tDCS condition (anodal, cathodal, sham), timepoint (t_0, t_{TDCS_5}, t_{TDCS_10}, t_{TDCS_15}, t_{TDCS_20}, t_{15}, t_{40}) and the visual stimulus direction (leftward, rightward) were included as fixed effect factors. To control for inter-individual variability of SP performance, subject ID was included as random effects factor (random intercept; identity covariance structure). tDCS condition, timepoint and ramp direction were considered as repeated factors (first-order autoregressive covariance structure). Main and interaction effects were analyzed in a saturated model. In case of specific tDCS effects (i.e., an interaction between tDCS condition, timepoint, and ramp direction), separate LMM analyses were computed for timepoints of online effects (t_{TDCS_5}, t_{TDCS_10}, t_{TDCS_15}, t_{TDCS_20}) and (after-)effects relative to t_0 (t_0, t_{TDCS}, t_{15}, t_{40}, using the averaged performance across all t_{TDCS} timepoints), further including tDCS condition and ramp direction as factors.

The significance level was set to α = .05 and post-hoc contrasts of estimated marginal means were computed for the highest-order interaction or main effect (Bonferroni-corrected for multiple comparisons). *F*-values and *p*-values are reported for significant main or interaction effects. For post-hoc tests, Bonferroni-corrected *p*-values, mean and standard error of the mean are reported. Effect sizes were estimated as the absolute value of Cohen's $d_z = \frac{t}{\sqrt{N}}$ with *N* being the respective sample size and *t* being the *t*-value computed based on the mean difference and standard error of the mean of the difference between estimated marginal means of the respective paired post-hoc contrast [95].

Furthermore, significant LMM tDCS condition * timepoint * stimulus direction interactions indicate specific tDCS effects. To follow-up these results in more detail, tDCS online effects were defined as the difference between the first and the last timepoint during t_{TDCS} (t_{TDCS_20} - t_{TDCS_5}) of the respective SP parameter, irrespective of the temporal evolution of this effect. A second, complementary estimate of tDCS effects was computed as the slope (*b*) of a robust linear regression computed across all timepoints during t_{TDCS} (t_{TDCS_5} to t_{TDCS_20}) assuming a quasi-linear evolution of the tDCS effect during the stimulation (Fig. 3). Both tDCS effect measures were compared between stimulus directions for each tDCS condition, as well as between tDCS conditions for each stimulus direction using bootstrapped paired *t*-tests (n = 10000 bootstrap samples were computed to determine the H_0 distribution). In addition, tDCS effects for the respective tDCS condition and stimulus direction were compared across experiments using bootstrapped paired *t*-tests to compare between experiment 1 (V5-personalized) versus experiment 2 (FEF-personalized) and unpaired *t*-tests to compare experiment 1 (V5-personalized) versus experiment 3 (V5-normative). For all bootstrap *t*-tests *z*-values and *p*-values (Bonferroni-corrected) are reported and Cohens d_z (paired contrast) or d_s (unpaired contrast) was computed based on the observed values [95].

Electric field simulations were compared between normative versus personalized tDCS montages. Individually simulated electric fields were interpolated on an MNI cortical surface representation and paired *t*-tests were computed for every position of the surface grid between personalized and normative tDCS (FDR-corrected) [96]. Furthermore, separate bootstrap paired *t*-test were computed (one-sided) with 10000 iterations using MATLAB (The Mathworks Ltd., MA/USA) for $|E|_{IT}$, $|E|_{DIR}$, and $|E|_{EXTENT}$. For each test, *z*-value, *p*-value and descriptive means and standard errors of the means are reported. Effect size d_z was estimated based on the observed values [95].

CRediT authorship contribution statement

Jan-Ole Radecke: Conceptualization, Methodology, Software, Investigation, Formal analysis, Writing - original draft, Visualization. **Alexander Kühn:** Investigation, Data curation, Formal Analysis, Writing – review & editing. **Tim Erdbrügger and Yvonne Buschermöhle:** Investigation, Methodology, Software, Writing - review & editing. **Sogand Rashidi and Hannah Stöckler:** Investigation, Data curation, Writing – review & editing. **Benjamin Sack:** Investigation, Writing - review & editing. **Stefan Borgwardt:** Resources, Supervision, Writing - review & editing. **Till R. Schneider:** Supervision, Methodology, Writing - review & editing. **Joachim Gross:** Supervision, Funding acquisition, Writing - review & editing. **Carsten H. Wolters:** Supervision, Project administration, Funding acquisition, Writing - review & editing. **Andreas Sprenger:** Methodology, Software, Supervision, Writing – review & editing. **Rebekka Lencer:** Project administration, Funding acquisition, Conceptualization, Writing - review & editing.

Acknowledgements

This work was supported by the German Research Foundation (DFG; WO1425/10-1 to CHW, GR2024/8-1 to JG and LE1122/7-1 to RL) and by the Bundesministerium für Gesundheit (BMG;

ZMI1-2521FSB006, under the frame of ERA PerMed as project ERAPERMED2020-227). JG was further supported by the DFG (GR2024/11-1, GR2024/12-1, TRR393). JOR was funded by the Clinician Scientist program of the Section of Medicine of the University of Lübeck. We thank Dr. Martin Göttlich and Andreas Wollbrink for technical support, Karin Wilken, Hildegard Deitermann, Ute Trompeter, Susanne Schellbach and Mandy-Josephine Reichhardt for support with the data acquisition, and Prof. Peter Trillenberg for helpful discussions.

References

1. Agtzidis, I., Meyhöfer, I., Dorr, M. & Lencer, R. Following Forrest Gump: Smooth pursuit related brain activation during free movie viewing. *Neuroimage* **216**, 116491 (2020).
2. Lisberger, S. G. Visual Guidance of Smooth-Pursuit Eye Movements: Sensation, Action, and What Happens in Between. *Neuron* **66**, 477–491 (2010).
3. Schutz, A. C., Braun, D. I. & Gegenfurtner, K. R. Eye movements and perception: A selective review. *J Vis* **11**, 9–9 (2011).
4. Lencer, R. & Trillenberg, P. Neurophysiology and neuroanatomy of smooth pursuit in humans. *Brain Cogn* **68**, 219–228 (2008).
5. Ilg, U. J. & Thier, P. The neural basis of smooth pursuit eye movements in the rhesus monkey brain. *Brain Cogn* **68**, 229–240 (2008).
6. Wilms, M. *et al.* Human V5/MT+: comparison of functional and cytoarchitectonic data. *Anat Embryol (Berl)* **210**, 485–495 (2005).
7. Ohlendorf, S. *et al.* Visual motion, eye motion, and relative motion: A parametric fMRI study of functional specializations of smooth pursuit eye movement network areas. *J Vis* **10**, 21–21 (2010).
8. Dukelow, S. P. *et al.* Distinguishing Subregions of the Human MT+ Complex Using Visual Fields and Pursuit Eye Movements. *J Neurophysiol* **86**, 1991–2000 (2001).
9. Komatsu, H. & Wurtz, R. H. Relation of cortical areas MT and MST to pursuit eye movements. I. Localization and visual properties of neurons. *J Neurophysiol* **60**, 580–603 (1988).
10. Komatsu, H. & Wurtz, R. H. Modulation of pursuit eye movements by stimulation of cortical areas MT and MST. *J Neurophysiol* **62**, 31–47 (1989).
11. Newsome, W. T., Wurtz, R. H. & Komatsu, H. Relation of cortical areas MT and MST to pursuit eye movements. II. Differentiation of retinal from extraretinal inputs. *J Neurophysiol* **60**, 604–620 (1988).
12. Lee, J., Joshua, M., Medina, J. F. & Lisberger, S. G. Signal, Noise, and Variation in Neural and Sensory-Motor Latency. *Neuron* **90**, 165–176 (2016).
13. Trillenberg, P. *et al.* Visual and non-visual motion information processing during pursuit eye tracking in schizophrenia and bipolar disorder. *Eur Arch Psychiatry Clin Neurosci* **267**, 225–235 (2017).
14. Sprenger, A. *et al.* The role of prediction and anticipation on age-related effects on smooth pursuit eye movements. *Ann N Y Acad Sci* **1233**, 168–176 (2011).
15. Helmchen, C. *et al.* Role of anticipation and prediction in smooth pursuit eye movement control in Parkinson's disease. *Movement Disorders* **27**, 1012–1018 (2012).
16. Lee, J., Darlington, T. R. & Lisberger, S. G. The Neural Basis for Response Latency in a Sensory-Motor Behavior. *Cerebral Cortex* **30**, 3055–3073 (2020).
17. Ferrera, V. P. Smooth pursuit preparation modulates neuronal responses in visual areas MT and MST. *J Neurophysiol* **114**, 638–649 (2015).
18. Lee, J. & Lisberger, S. G. Gamma Synchrony Predicts Neuron–Neuron Correlations and Correlations with Motor Behavior in Extrastriate Visual Area MT. *The Journal of Neuroscience* **33**, 19677–19688 (2013).
19. Newsome, W., Wurtz, R., Dursteler, M. & Mikami, A. Deficits in visual motion processing following ibotenic acid lesions of the middle temporal visual area of the macaque monkey. *The Journal of Neuroscience* **5**, 825–840 (1985).
20. Newsome, W. & Wurtz, R. Probing visual cortical function with discrete chemical lesions. *Trends Neurosci* **11**, 394–400 (1988).
21. Dursteler, M. R. & Wurtz, R. H. Pursuit and optokinetic deficits following chemical lesions of cortical areas MT and MST. *J Neurophysiol* **60**, 940–965 (1988).
22. Dursteler, M. R., Wurtz, R. H. & Newsome, W. T. Directional pursuit deficits following lesions of the foveal representation within the superior temporal sulcus of the macaque monkey. *J Neurophysiol* **57**, 1262–1287 (1987).

23. Heide, W., Kurzidim, K. & Kömpf, D. Deficits of smooth pursuit eye movements after frontal and parietal lesions. *Brain* **119**, 1951–1969 (1996).
24. Sharpe, J. A. Neurophysiology and neuroanatomy of smooth pursuit: Lesion studies. *Brain Cogn* **68**, 241–254 (2008).
25. Thurston, S. E., Leigh, R. J., Crawford, T., Thompson, A. & Kennard, C. Two distinct deficits of visual tracking caused by unilateral lesions of cerebral cortex in humans. *Ann Neurol* **23**, 266–273 (1988).
26. Haarmeier, T. & Kammer, T. Effect of TMS on Oculomotor Behavior but not Perceptual Stability during Smooth Pursuit Eye Movements. *Cerebral Cortex* **20**, 2234–2243 (2010).
27. Nagel, M., Sprenger, A., Hohagen, F., Binkofski, F. & Lencer, R. Cortical mechanisms of retinal and extraretinal smooth pursuit eye movements to different target velocities. *Neuroimage* **41**, 483–492 (2008).
28. Nagel, M., Sprenger, A., Steinlechner, S., Binkofski, F. & Lencer, R. Altered Velocity Processing in Schizophrenia during Pursuit Eye Tracking. *PLoS One* **7**, e38494 (2012).
29. Lencer, R., Nagel, M., Sprenger, A., Heide, W. & Binkofski, F. Reduced neuronal activity in the V5 complex underlies smooth-pursuit deficit in schizophrenia: evidence from an fMRI study. *Neuroimage* **24**, 1256–1259 (2005).
30. Radecke, J.-O. *et al.* Normative tDCS over V5 and FEF reveals practice-induced modulation of extraretinal smooth pursuit mechanisms, but no specific stimulation effect. *Sci Rep* **13**, 21380 (2023).
31. Knox, P. C., Davidson, J. H. & Anderson, D. Age-related changes in smooth pursuit initiation. *Exp Brain Res* **165**, 1–7 (2005).
32. Campion, D. *et al.* SPEM impairment in drug-naive schizophrenic patients: Evidence for a trait marker. *Biol Psychiatry* **32**, 891–902 (1992).
33. Lencer, R. *et al.* Smooth pursuit performance in families with multiple occurrence of schizophrenia and nonpsychotic families. *Biol Psychiatry* **45**, 694–703 (1999).
34. Lencer, R. *et al.* Pursuit eye movements as an intermediate phenotype across psychotic disorders: Evidence from the B-SNIP study. *Schizophr Res* **169**, 326–333 (2015).
35. Meyhoefer, I. *et al.* Evidence from comprehensive independent validation studies for smooth pursuit dysfunction as a sensorimotor biomarker for psychosis. *Sci Rep* **14**, 13859 (2024).
36. Kar, K. & Krekelberg, B. Transcranial Alternating Current Stimulation Attenuates Visual Motion Adaptation. *Journal of Neuroscience* **34**, 7334–7340 (2014).
37. Antal, A. *et al.* Facilitation of visuo-motor learning by transcranial direct current stimulation of the motor and extrastriate visual areas in humans. *European Journal of Neuroscience* **19**, 2888–2892 (2004).
38. Antal, A. *et al.* Direct Current Stimulation over V5 Enhances Visuomotor Coordination by Improving Motion Perception in Humans. *J Cogn Neurosci* **16**, 521–527 (2004).
39. Antal, A. *et al.* Direct current stimulation over MT + /V5 modulates motion aftereffect in humans. *Neuroreport* **15**, 2491–2494 (2004).
40. Antal, A. *et al.* Cathodal stimulation of human MT+ leads to elevated fMRI signal: A tDCS-fMRI study. *Restor Neurol Neurosci* **30**, 255–263 (2012).
41. Battaglini, L., Noventa, S. & Casco, C. Anodal and cathodal electrical stimulation over V5 improves motion perception by signal enhancement and noise reduction. *Brain Stimul* **10**, 773–779 (2017).
42. Wiethoff, S., Hamada, M. & Rothwell, J. C. Variability in response to transcranial direct current stimulation of the motor cortex. *Brain Stimul* **7**, 468–475 (2014).
43. Tremblay, S. *et al.* Systematic assessment of duration and intensity of anodal transcranial direct current stimulation on primary motor cortex excitability. *European Journal of Neuroscience* **44**, 2184–2190 (2016).
44. López-Alonso, V., Cheeran, B., Río-Rodríguez, D. & Fernández-Del-Olmo, M. Inter-individual variability in response to non-invasive brain stimulation paradigms. *Brain Stimul* **7**, 372–380 (2014).
45. Dedoncker, J., Brunoni, A. R., Baeken, C. & Vanderhasselt, M.-A. A Systematic Review and Meta-Analysis of the Effects of Transcranial Direct Current Stimulation (tDCS) Over the Dorsolateral Prefrontal Cortex in Healthy and Neuropsychiatric Samples: Influence of Stimulation Parameters. *Brain Stimul* **9**, 501–517 (2016).
46. Schutter, D. J. L. G. & Wischnewski, M. A meta-analytic study of exogenous oscillatory electric potentials in neuroenhancement. *Neuropsychologia* **86**, 110–118 (2016).
47. Gomez-Tames, J. & Fernández-Corazza, M. Perspectives on Optimized Transcranial Electrical Stimulation Based on Spatial Electric Field Modeling in Humans. *J Clin Med* **13**, 3084 (2024).
48. Alekseichuk, I., Wischnewski, M. & Opitz, A. A minimum effective dose for (transcranial) alternating current stimulation. *Brain Stimul* **15**, 1221–1222 (2022).

49. Wischnewski, M., Alekseichuk, I. & Opitz, A. Neurocognitive, physiological, and biophysical effects of transcranial alternating current stimulation. *Trends Cogn Sci* **27**, 189–205 (2023).
50. Esmaeilpour, Z. *et al.* Incomplete evidence that increasing current intensity of tDCS boosts outcomes. *Brain Stimul* **11**, 310–321 (2018).
51. Kasten, F. H., Duecker, K., Maack, M. C., Meiser, A. & Herrmann, C. S. Integrating electric field modeling and neuroimaging to explain inter-individual variability of tACS effects. *Nat Commun* **10**, 5427 (2019).
52. Johnson, L. *et al.* Dose-dependent effects of transcranial alternating current stimulation on spike timing in awake nonhuman primates. *Sci Adv* **6**, eaaz2747 (2020).
53. Antonenko, D. *et al.* Towards precise brain stimulation: Is electric field simulation related to neuromodulation? *Brain Stimul* **12**, 1159–1168 (2019).
54. Radecke, J.-O. *et al.* Personalized alpha-tACS targeting left posterior parietal cortex modulates visuo-spatial attention and posterior evoked EEG activity. *Brain Stimul* **16**, 1047–1061 (2023).
55. Caulfield, K. A. *et al.* Transcranial electrical stimulation motor threshold can estimate individualized tDCS dosage from reverse-calculation electric-field modeling. *Brain Stimul* **13**, 961–969 (2020).
56. Wischnewski, M., Mantell, K. E. & Opitz, A. Identifying regions in prefrontal cortex related to working memory improvement: A novel meta-analytic method using electric field modeling. *Neurosci Biobehav Rev* **130**, 147–161 (2021).
57. Gross, J., Junghöfer, M. & Wolters, C. H. Bioelectromagnetism in Human Brain Research: New Applications, New Questions. *The Neuroscientist* 107385842110547 (2021) doi:10.1177/10738584211054742.
58. Liu, A. *et al.* Immediate neurophysiological effects of transcranial electrical stimulation. *Nat Commun* **9**, (2018).
59. Polanía, R., Nitsche, M. A. & Ruff, C. C. Studying and modifying brain function with non-invasive brain stimulation. *Nat Neurosci* **21**, 174–187 (2018).
60. Evans, C. *et al.* Dose-controlled tDCS reduces electric field intensity variability at a cortical target site. *Brain Stimul* **13**, 125–136 (2020).
61. Radecke, J.-O., Khan, A., Engel, A. K., Wolters, C. H. & Schneider, T. R. Individual Targeting Increases Control Over Inter-Individual Variability in Simulated Transcranial Electric Fields. *IEEE Access* **8**, 182610–182624 (2020).
62. Khan, A. *et al.* Can individually targeted and optimized multi-channel tDCS outperform standard bipolar tDCS in stimulating the primary somatosensory cortex? *Brain Stimul* **16**, 1–16 (2023).
63. Mohd Zulkifly, M. F. *et al.* Directionality of the injected current targeting the P20/N20 source determines the efficacy of 140 Hz transcranial alternating current stimulation (tACS)-induced aftereffects in the somatosensory cortex. *PLoS One* **17**, e0266107 (2022).
64. Cabral-Calderin, Y., van Hinsberg, D., Thielscher, A. & Henry, M. J. Behavioral entrainment to rhythmic auditory stimulation can be modulated by tACS depending on the electrical stimulation field properties. *Elife* **12**, (2024).
65. Lencer, R. *et al.* Cortical mechanisms of smooth pursuit eye movements with target blanking. An fMRI study. *European Journal of Neuroscience* **19**, 1430–1436 (2004).
66. Tzourio-Mazoyer, N. *et al.* Automated Anatomical Labeling of Activations in SPM Using a Macroscopic Anatomical Parcellation of the MNI MRI Single-Subject Brain. *Neuroimage* **15**, 273–289 (2002).
67. Wild, B. & Treue, S. Primate extrastriate cortical area MST: a gateway between sensation and cognition. *J Neurophysiol* **125**, 1851–1882 (2021).
68. Maunsell, J. & van Essen, D. The connections of the middle temporal visual area (MT) and their relationship to a cortical hierarchy in the macaque monkey. *The Journal of Neuroscience* **3**, 2563–2586 (1983).
69. Boussaoud, D., Desimone, R. & Ungerleider, L. G. Subcortical connections of visual areas MST and FST in macaques. *Vis Neurosci* **9**, 291–302 (1992).
70. Kimmig, H. *et al.* fMRI evidence for sensorimotor transformations in human cortex during smooth pursuit eye movements. *Neuropsychologia* **46**, 2203–2213 (2008).
71. Barnes, G. R. Cognitive processes involved in smooth pursuit eye movements. *Brain Cogn* **68**, 309–326 (2008).
72. Becker, W. & Fuchs, A. F. Prediction in the oculomotor system: smooth pursuit during transient disappearance of a visual target. *Exp Brain Res* **57**, 562–575 (1985).
73. Nitsche, M. A. & Paulus, W. Excitability changes induced in the human motor cortex by weak transcranial direct current stimulation. *J Physiol* **527**, 633–639 (2000).
74. Krause, M. R. *et al.* Transcranial Direct Current Stimulation Facilitates Associative Learning and Alters Functional Connectivity in the Primate Brain. *Current Biology* **27**, 3086-3096.e3 (2017).

75. Creutzfeldt, O. D., Fromm, G. H. & Kapp, H. Influence of transcortical d-c currents on cortical neuronal activity. *Exp Neurol* **5**, 436–452 (1962).
76. Jamil, A. *et al.* Current intensity- and polarity-specific online and aftereffects of transcranial direct current stimulation: An fMRI study. *Hum Brain Mapp* **41**, 1644–1666 (2020).
77. Bachtiar, V., Near, J., Johansen-Berg, H. & Stagg, C. J. Modulation of GABA and resting state functional connectivity by transcranial direct current stimulation. *Elife* **4**, (2015).
78. Stagg, C. J. *et al.* Polarity-Sensitive Modulation of Cortical Neurotransmitters by Transcranial Stimulation. *The Journal of Neuroscience* **29**, 5202–5206 (2009).
79. Antonenko, D. *et al.* tDCS-Induced Modulation of GABA Levels and Resting-State Functional Connectivity in Older Adults. *The Journal of Neuroscience* **37**, 4065–4073 (2017).
80. Liebetanz, D., Nitsche, M. A., Tergau, F. & Paulus, W. Pharmacological approach to the mechanisms of transcranial DC-stimulation-induced after-effects of human motor cortex excitability. *Brain* **125**, 2238–2247 (2002).
81. Nitsche, M. A. *et al.* Pharmacological Modulation of Cortical Excitability Shifts Induced by Transcranial Direct Current Stimulation in Humans. *J Physiol* **553**, 293–301 (2003).
82. Kuo, H.-I. *et al.* Acute and Chronic Noradrenergic Effects on Cortical Excitability in Healthy Humans. *International Journal of Neuropsychopharmacology* **20**, 634–643 (2017).
83. Furuya, S., Klaus, M., Nitsche, M. A., Paulus, W. & Altenmüller, E. Ceiling Effects Prevent Further Improvement of Transcranial Stimulation in Skilled Musicians. *The Journal of Neuroscience* **34**, 13834–13839 (2014).
84. Bestmann, S., de Berker, A. O. & Bonaiuto, J. Understanding the behavioural consequences of noninvasive brain stimulation. *Trends Cogn Sci* **19**, 13–20 (2015).
85. Khan, A., Antonakakis, M., Vogenauer, N., Haueisen, J. & Wolters, C. H. Individually optimized multi-channel tDCS for targeting somatosensory cortex. *Clinical Neurophysiology* **134**, 9–26 (2022).
86. Lefaucheur, J.-P. *et al.* Evidence-based guidelines on the therapeutic use of transcranial direct current stimulation (tDCS). *Clinical Neurophysiology* **128**, 56–92 (2017).
87. Fregni, F. *et al.* Evidence-Based Guidelines and Secondary Meta-Analysis for the Use of Transcranial Direct Current Stimulation in Neurological and Psychiatric Disorders. *International Journal of Neuropsychopharmacology* **24**, 256–313 (2021).
88. Soleimani, G., Kupliki, R., Bodurka, J., Paulus, M. P. & Ekhtiari, H. How structural and functional MRI can inform dual-site tACS parameters: A case study in a clinical population and its pragmatic implications. *Brain Stimul* **15**, 337–351 (2022).
89. Buschermöhle, Y. *et al.* Comparing the performance of beamformer algorithms in estimating orientations of neural sources. *iScience* **27**, 109150 (2024).
90. Antonakakis, M. *et al.* Inter-Subject Variability of Skull Conductivity and Thickness in Calibrated Realistic Head Models. *Neuroimage* **223**, 117353 (2020).
91. Schrader, S., Antonakakis, M., Rampp, S., Engwer, C. & Wolters, C. H. A novel method for calibrating head models to account for variability in conductivity and its evaluation in a sphere model. *Phys Med Biol* **65**, 245043 (2020).
92. Vieira, P., Krause, M. & Pack, C. tACS entrains neural activity while somatosensory input is blocked. (2019) doi:10.1101/691022.
93. Misselhorn, J., Fiene, M., Radecke, J.-O., Engel, A. K. & Schneider, T. R. Transcranial Alternating Current Stimulation over Frontal Eye Fields Mimics Attentional Modulation of Visual Processing. *The Journal of Neuroscience* **44**, e1510232024 (2024).
94. Rashbass, C. The relationship between saccadic and smooth tracking eye movements. *J Physiol* **159**, 326–338 (1961).
95. Lakens, D. Calculating and reporting effect sizes to facilitate cumulative science: a practical primer for t-tests and ANOVAs. *Front Psychol* **4**, (2013).
96. Benjamini, Y. & Hochberg, Y. Controlling the false discovery rate: a practical and powerful approach to multiple testing. *Journal of the Royal Statistical Society* vol. 57 289–300 Preprint at https://doi.org/10.2307/2346101 (1995).
97. Beck, A. T., Steer, R. A. & Brown, G. K. *Manual for Beck Depression Inventory-II*. (Psychological Corporation, San Antonio, TX, 1996).
98. Lehrl, S. *Mehrfachwahl-Wortschatz-Intelligenztest MWT-B [Multiple Choice Vocabulary Test, Version B]*. (Spitta, Balingen, 2005).

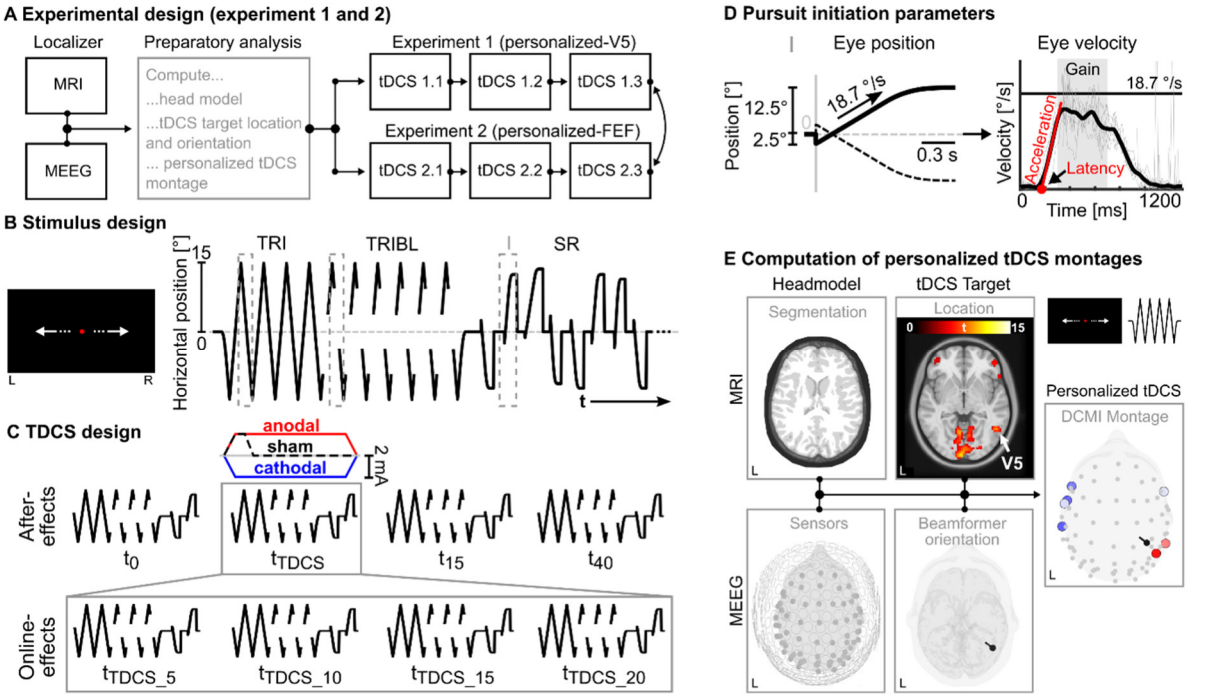

Figure 1. Experimental design. A) Personalized tDCS in experiment 1 and 2 comprised eight experimental sessions on separate days per participant (black boxes). During the first two appointments participants completed MRI and MEEG localizer experiments. Localizer data was used to compute personalized tDCS montages (gray box). Sham, anodal, and cathodal tDCS was applied in three subsequent sessions targeting V5 or FEF. After participants completed the first experiment, three further tDCS sessions were completed for the respective second experiment. The initial assignment to experiment 1 or 2, as well as the order of sham, anodal, and cathodal tDCS within each experiment was counterbalanced across participants. **B)** Horizontally moving visual stimuli were presented. To evaluate the effect of personalized tDCS on different aspects of SP, three tasks were presented, namely continuous SP (TRI), continuous SP with blanking (TRIBL), and foveopetal step-ramp stimuli (I, SR). **C)** In each tDCS session, SP tasks were presented before (t_0), at four timepoints during (t_{TDCS_5}, t_{TDCS_10}, t_{TDCS_15}, t_{TDCS_20}), and 15 (t_{15}) or 40 minutes (t_{40}) after tDCS application. **D)** Pursuit initiation parameters were computed based on the eye tracking data recorded during the step-ramp task. Eye velocities (right) were derived from the eye position (left) as a function of time. Pursuit latency and initial acceleration were computed to define open-loop SP initiation performance. Early gain was computed to estimate closed-loop performance (300 to 700 ms after target motion onset). Target velocity is indicated by a black line at 18.7 °/s. **E)** To compute personalized tDCS montages, structural MRI data were acquired to create a six-compartment segmentation of the individual head (top left). Together with the sensor positions from the combined MEEG session (bottom left), as well as individually calibrated skull conductivity and white matter anisotropy (not shown) individual FEM head models were computed. Individual tDCS targets were defined, using functional MRI data acquired during continuous SP to define the target location in the right hemisphere (top middle, MNI z = -4), and combined MEEG data to define the target orientation (bottom middle). Together the head model and tDCS target information were used to compute personalized tDCS montages with the DCMI algorithm. The workflow to target the area V5 is shown for one exemplary subject.

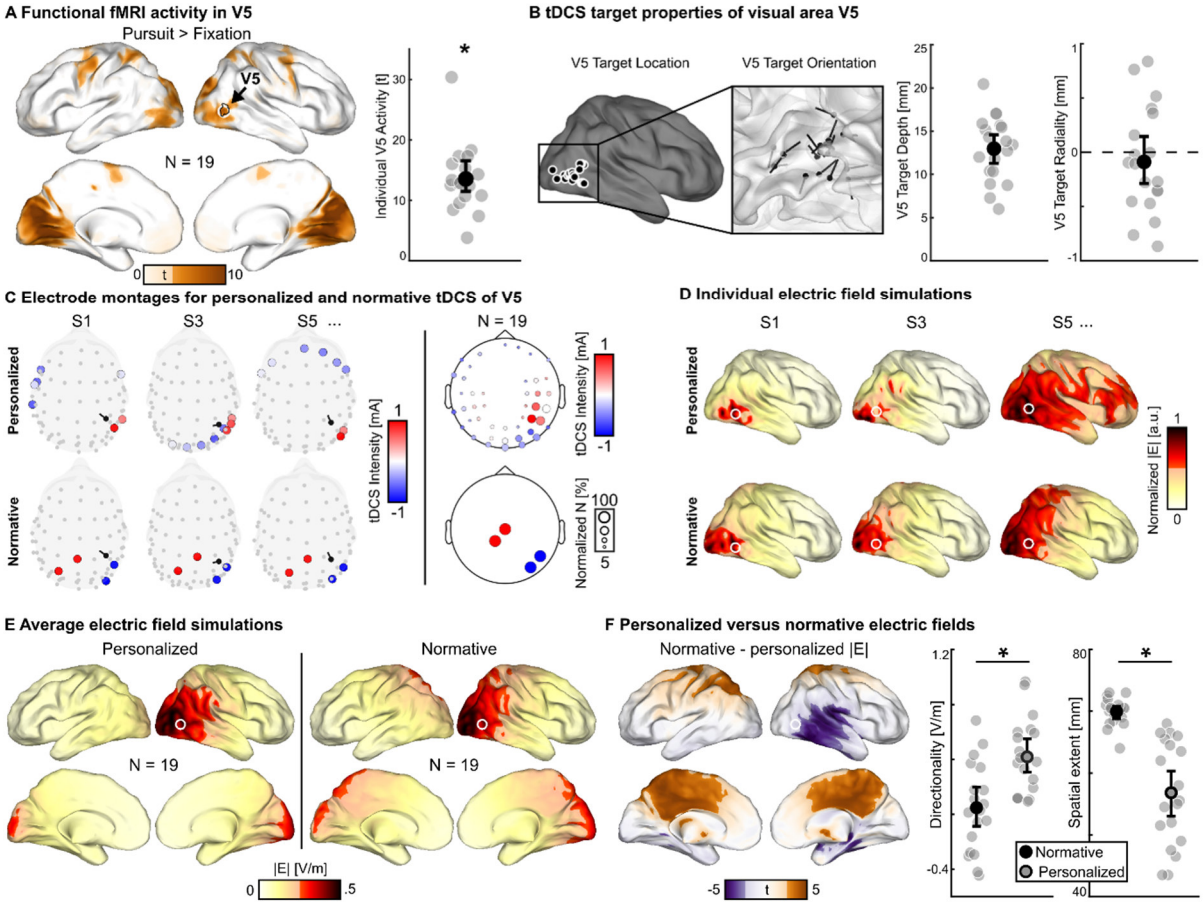

Figure 2. Target V5 and personalized transcranial electric fields. A) Left: Second-level BOLD activity during ongoing SP, compared to fixation, revealed a significant cluster that corresponds to visual area V5. The V5-equivalent cytoarchitectonic area hOc5 (black lines) corresponds to the average coordinate of individual V5 estimates (white circle). FDR-corrected *t*-values are shown, interpolated on the inflated cortical surface of the MNI brain. Right: Individual target V5 activity. Bootstrap mean and confidence interval is depicted together with individual local maxima *t*-values of the first-level statistical contrast of BOLD activity during ongoing SP, compared to fixation. **B)** Target V5 locations (left) are shown on an inflated cortical surface of the MNI brain. Estimated V5 orientations (middle) are shown together with the white matter surface of the MNI brain. Right: V5 target depth relative to the inner skull surface and radiality (1/-1 = radial/anti-radial, 0 = tangential) bootstrap means and confidence intervals are depicted together with individual values. **C)** Personalized tDCS montages targeting individual V5 (top) and normative tDCS montages over V5 (bottom) are shown for three exemplary subjects (left; top view). Topographical representations for the whole sample are shown for personalized (top right) and normative tDCS montages (bottom right). Circle sizes illustrate the normalized number of individual montages that comprised the respective electrode, color illustrates the average tDCS intensity per electrode across the whole sample. **D)** Electric field simulations for the same three subjects and personalized (top) and normative (bottom) tDCS montages, respectively. Normalized electric field intensities |**E**| were interpolated on the inflated right cortical surface of the MNI brain, with values below 50% of the maximal intensity masked (light colors). Individual tDCS target locations in the right V5 are indicated by white circles. **E)** Lateral and medial view of average simulated electric fields for personalized (left) and normative (right) tDCS interpolated on the inflated cortical surface of the MNI brain, with values below 50% of the maximal intensity masked (light colors). The average tDCS target location in the right V5 is indicated by a white circle, respectively. **F)** Left: Comparison between personalized and normative simulated electric fields revealed increased electric field intensities in bilateral parietal and medial brain regions for normative tDCS, whereas personalized electric field intensities were increased in right temporal, and parietal regions anterior to the average V5 location (white circle), corresponding to more anterior individual V5 locations (compare panel B). Lateral and medial view of significant *t*-values are shown (bold colors), with *t*-values corresponding to FDR-corrected *p*-values > 0.05 masked (light colors). Right: Directionalities in the target V5 for electric fields induced by normative tDCS were significantly smaller and spatial extent of the electric field across the cortex was significantly larger, compared to personalized target directionalities and spatial extent. Bootstrap means and confidence intervals are depicted together with individual values. * indicate $p < .05$.

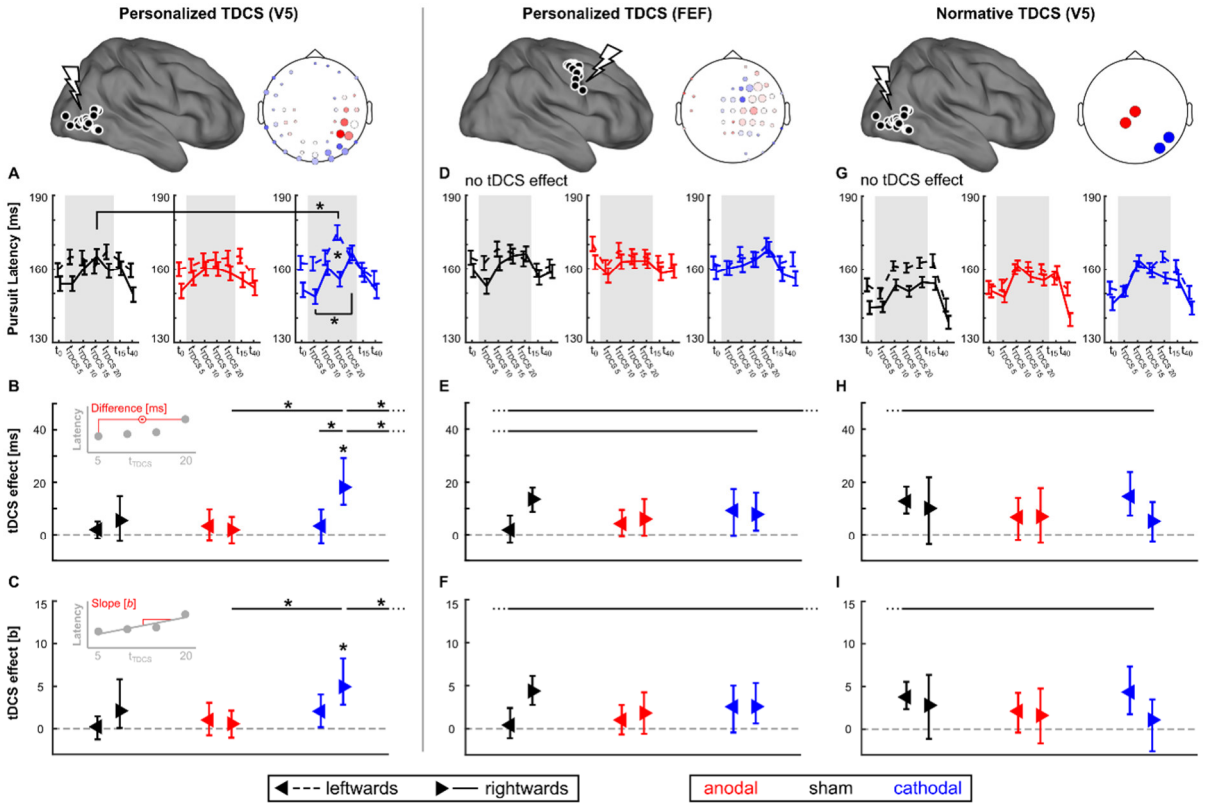

Figure 3. tDCS effects on SP latencies during the step-ramp task. A) to C) In experiment 1 (V5-personalized), significant modulation of SP latencies during the SR task by personalized cathodal tDCS targeting V5 was observed. An effect was observed across **A)** all timepoints (t_0, t_{TDCS_5}, t_{TDCS_10}, t_{TDCS_15}, t_{TDCS_20}, t_{15}, t_{40}). Gray shaded boxes indicate the 20 minutes tDCS interval. LMM analyses revealed an online effect of personalized cathodal tDCS with significantly delayed latencies for ipsiversive (i.e., rightwards) SP during the last timepoint (t_{TDCS_20}), compared to the first (t_{TDCS_5}) timepoint during t_{TDCS}. **B)** tDCS effect estimated as difference between t_{TDCS_20} versus t_{TDCS_5} is plotted for sham, anodal, and cathodal tDCS conditions, as well as leftwards and rightwards SP latencies, respectively (bootstrap mean ± confidence interval). Top left inset illustrates the computation of the difference tDCS effect. Follow-up analysis of difference tDCS effects reveals significant differences for personalized cathodal tDCS for rightward SP latencies, compared to leftward SP latencies of the same tDCS condition, rightward SP latencies during anodal tDCS, as well as an increased difference tDCS effect of personalized cathodal tDCS targeting V5, compared to personalized tDCS targeting FEF and normative cathodal tDCS over V5. **C)** tDCS effect estimated as slope of robust regression across all t_{TDCS} timepoints is plotted for sham, anodal, and cathodal tDCS conditions, as well as leftwards and rightwards SP latencies, respectively (bootstrap mean ± confidence interval). Top left inset illustrates the computation of the slope tDCS effect. Slope estimates of tDCS effects are significantly increased for personalized cathodal tDCS targeting V5, compared to anodal tDCS, as well as normative cathodal tDCS over V5. **D) to F)** No specific tDCS effects were observed for personalized tDCS targeting the right FEF. **G) to I)** No specific tDCS effects were observed for normative tDCS over the right V5. * indicate $p < .05$ (Bonferroni-corrected). tDCS targets and topographical illustration of the cathodal tDCS montage are depicted for the experiment 1 (V5-personalized, top left), experiment 2 (FEF-personalized, top middle), and experiment 3 (V5-normative, top right), respectively.

Table 1. Sample information for the personalized and the normative tDCS participants. For both samples sample size (N), age (M ± SD), gender (frequencies), handedness (frequencies), raw values for the Beck Depression Inventory (BDI-II 126) and percentile ranks for the Multiple Choice Vocabulary Test (MWT-B 127) are provided. F = female, M = male, R = right-handed, L = left-handed, A = ambidextrous.

Parameter	Personalized tDCS targeting V5 and FEF	Normative tDCS over V5
Sample size	19	19
Age	26.2 ± 7.6	25.5 ± 7.1
Gender	F: 11, M: 8	F: 11, M: 8
Handedness	R: 16, L: 2, A: 1	R: 16, L: 3
BDI-II	1.7 ± 2.2	1.4 ± 1.2
MWT-B	47.7 ± 19.6	55.2 ± 20
Days between tDCS sessions	7.9 ± 7.8	8.5 ± 4.7

Table 2. Descriptive smooth pursuit performance. Great grand average pursuit performance for experiment 1 (V5-personalized), experiment 2 (FEF-personalized), and experiment 3 (V5-normative). Mean (± SD) is reported for the respective parameters of continuous pursuit (TRI), continuous pursuit with blanking (TRIBL), and foveopetal step-ramps (SR). a.u. = arbitrary unit.

Task	Parameter	Unit	Experiment 1 (V5-personalized)	Experiment 2 (FEF-personalized)	Experiment 3 (V5-normative)
TRI	Maintenance gain	a.u.	0.957 ± 0.042	0.936 ± 0.044	0.941 ± 0.039
TRIBL	Preblank gain	a.u.	0.839 ± 0.108	0.819 ± 0.108	0.814 ± 0.112
	Deceleration latency	ms	130 ± 17	134 ± 22	134 ± 19
	Deceleration	$°/s^2$	47 ± 9	46 ± 9	54 ± 7
	Resdidual gain	a.u.	0.439 ± 0.223	0.425 ± 0.216	0.314 ± 0.145
	Re-acceleration latency	ms	-132 ± 35	-136 ± 39	-136 ± 39
	Re-acceleration	$°/s^2$	27 ± 10	26 ± 10	26 ± 9
	Postblank gain	a.u.	0.811 ± 0.125	0.786 ± 0.106	0.731 ± 0.145
SR	Pursuit latency	ms	160 ± 13	163 ± 13	154 ± 11
	Acceleration	$°/s^2$	128 ± 34	126 ± 33	109 ± 29
	Early maintenance gain	a.u.	0.827 ± 0.086	0.809 ± 0.087	0.799 ± 0.094

Table 3. Personalized tDCS targeting V5 induces online effects modulating SP initiation. Results of LMM analysis indicate significant transient modulation of SP initiation, specifically pursuit latency and initial acceleration during SR, by personalized tDCS targeting V5 during the tDCS application (online effects, i.e. considering timepoints t_{TDCS_5}, t_{TDCS_10}, t_{TDCS_15}, and t_{TDCS_20}). TRI = continuous pursuit, TRIBL = continuous pursuit with blanking, SR = step-ramp. * indicate *p*-values < .05.

Task	Parameter	tDCS condition		tDCS condition * Timepoint		tDCS condition * Direction		tDCS condition * Timepoint * Direction	
		F	*p*	F	*p*	F	*p*	F	*p*
TRI	Maintenance gain	1.35	.263	0.26	*.955*	1.71	*.183*	0.63	*.705*
TRIBL	Preblank gain	**6.09 ***	***.003***	1.31	*.252*	0.55	*.58*	0.28	*.948*
	Deceleration latency	1.59	.207	0.19	*.98*	1.37	*.257*	0.28	*.945*
	Deceleration	2.61	.077	0.15	*.989*	0.12	*.886*	0.86	*.521*
	Residual gain	0.32	.73	0.26	*.955*	0.54	*.586*	0.11	*.995*
	Re-acceleration latency	**4.79 ***	***.01***	0.7	*.648*	0.77	*.467*	1.1	*.36*
	Re-acceleration	0.02	.978	0.28	*.945*	0.39	*.675*	0.59	*.736*
	Postblank gain	**3.24 ***	***.041***	0.39	*.887*	0.02	*.982*	0.46	*.836*
SR	Pursuit latency	0.63	.534	1.11	*.355*	0.79	*.456*	**2.7 ***	***.015***
	Initial acceleration	0.29	.751	0.77	*.596*	0.25	*.78*	**2.56 ***	***.02***
	Early maintenance gain	**4.74 ***	***.01***	0.41	*.87*	0.15	*.862*	0.74	*.62*

Table 4. No tDCS after-effects. Results of LMM analysis do not indicate a significant modulation of SP parameters after personalized tDCS targeting V5 (after effects, i.e. considering timepoints t_0, t_{15}, and t_{40}). TRI = continuous pursuit, TRIBL = continuous pursuit with blanking, SR = step-ramp. * indicate *p*-values < .05.

Task	Parameter	tDCS condition		tDCS condition * Timepoint		tDCS condition * Direction		tDCS condition * Timepoint * Direction	
		F	*p*	F	*p*	F	p	F	*p*
TRI	Maintenance gain	0.71	*.491*	1.56	*.159*	0.05	*.954*	0.19	*.979*
TRIBL	Preblank gain	0.45	*.638*	1.19	*.312*	1	*.369*	0.46	*.838*
	Deceleration latency	0.87	*.42*	0.58	*.748*	0.06	*.943*	0.9	*.492*
	Deceleration	0.18	*.836*	0.37	*.896*	0.92	*.4*	0.31	*.934*
	Residual gain	0.51	*.599*	0.27	*.95*	0.1	*.902*	0.15	*.99*
	Re-acceleration latency	**6.7 ***	***.002***	1.94	*.074*	0.08	*.924*	0.54	*.782*
	Re-acceleration	0.44	*.644*	0.11	*.995*	0.62	*.542*	1.42	*.207*
	Postblank gain	1.34	*.264*	1.14	*.342*	0.04	*.963*	0.15	*.989*
SR	Pursuit latency	0.72	*.487*	0.53	*.786*	0.07	*.936*	0.92	*.484*
	Initial acceleration	0.28	*.755*	0.48	*.824*	0.01	*.989*	0.43	*.857*
	Early maintenance gain	1.36	*.259*	0.83	*.545*	0.24	*.784*	0.14	*.991*